Pramana – J. Phys. (2020) 94:40
https://doi.org/10.1007/s12043-019-1905-1

The influence of two kinds of time delays on the vibrational resonance of a fractional Mathieu–Duffing oscillator

LIJUAN NING* and WEN GUO

School of Mathematics and Information Science, Shaanxi Normal University, Xi'an, China
*Corresponding author. E-mail: ninglijuan@snnu.edu.com

MS received 28 August 2019; revised 18 October 2019; accepted 24 November 2019

Abstract. Vibrational resonance is studied in a fractional Mathieu–Duffing oscillator with two types of time delays: fixed and distributed delays. The theoretical expression of the response amplitude is obtained by utilising the method of direct partition of slow and fast motions. Relative errors between the theoretical prediction and the numerical simulation are introduced to verify the validity of analytical approaches. The relative error of the displacement and the relative error of the response amplitude are calculated. Small relative errors show that the theoretical analysis is statistically correct. Therefore, the effects of fractional order, linear stiffness coefficient, low-frequency signal, time delay intensity and damping coefficient on the Mathieu–Duffing oscillator with distributed delay are studied successively. In order to better illustrate the impact of distributed time delay on the model, the case of fixed time delay is analysed and compared, and it can be found that the distributed delay has more significant influence than fixed delay on the system. In addition, the influence of distributed delay on the system is more significant than that of the fixed delay.

Keywords. Fractional Mathieu–Duffing oscillator; distributed delay; fixed time delay; relative error.

PACS Nos **12.60.Jv; 12.10.Dm; 98.80.Cq; 11.30.Hv**

1. Introduction

The advent of stochastic resonance (SR) has led to the recognition of the active effects of noise. Benzi *et al* [1] proposed the concept of SR, which confirmed the positive influence of noise on the system output [2,3]. When the noise is replaced by a high-frequency signal in the system where SR occurs, a phenomenon similar to SR is found, which is known as vibrational resonance (VR) [4–6]. VR, which focusses on how to amplify weak low-frequency signals with another deterministic high-frequency signal, is more controllable. After the seminal paper by Landa and McClintock [7], there are huge volumes of literatures in VR, for example the neural network system [8–10], an analogy electrical circuits [11], vertical cavity laser systems [5], FitzHugh–Nagumo neuronal model [12,13], a genetic toggle-switch [14], an optical system [5,15], coupled systems [16,17], acoustics [18] and so on.

In complex media such as glasses, liquid crystals, polymers and biopolymers, the dynamical variable of interest often obeys fractional differential equations [19]. Compared to integer-order systems, the most significant advantage of fractional derivative equations is the storage characteristic. Hence, in recent years, the exploration of fractional-order systems has attracted extensive attention, and has been widely investigated in numerous scientific and engineering fields [20–32]. In view of the advantages of better control accuracy, better robustness and strong antinoise ability, it can be artificially introduced to control the system. Without loss of generality, here we consider damping as fractional order to achieve control of VR, and this is one of our motivations.

Parametric excitation which is ubiquitous is often used to model different phenomena in many fields of science and engineering [33–40]. Parametric excitations usually exist in high-frequency forms [41–47]. In addition to fast parametric excitation, there may be other slow excitations acting on physical or mechanical structures. Although slow excitation is usually weak, it often represents characteristic information in some cases. Scholars expressed a keen interest in the response. The Mathieu–Duffing oscillator, which is a

Published online: 10 February 2020

typical parametric excitation system, deserves to be studied. Taking such a system with fractional order as a model, it is our goal to explore the response of fractional order to slow changes in low frequencies. Besides, time delay, which exists in most of the real natural systems, can induce many rich dynamic behaviours, such as resonance, bifurcation and chaos. The dynamic behaviours of different models with time delay have become a hot topic. Overwhelming majority of previous literatures considers time delay as fixed constants, which is not entirely correct. Actually, it is not possible to maintain time delay as constant. It is more reasonable to regard it as a random number obeying a certain distribution where it is called distributed time delay. In [48,49], a logistic model with distributed delay is investigated and many meaningful phenomena are found. The delayed damped Mathieu equation, a second-order differential equation with periodic coefficients, is widely applied for analysing and modelling a large variety of practical systems [50]. We wonder what is the dynamic mechanism in such systems with the fractional order and distributed time delay.

In the previous papers, there is not much research on fractional order type VR, let alone the study of VR in a time-delay model. Stimulated by the above discussion, we can think about two kinds of time delays: the fixed time delay and the distributed delay. In the present work, we explore the VR of a fractional-order Mathieu–Duffing oscillator under two types of delays by using the method of separation of slow and fast motions. The remainder of this paper is organised as follows. Section 2 mainly discusses the model and theoretical description of VR, both the theoretical prediction and numerical simulation in a fractional Mathieu–Duffing oscillator with the distributed delay. In §3, we give the theoretical description of the fractional Mathieu–Duffing oscillator with fixed delay. The resonance analysis of two kinds of time-delay systems are discussed. Also the errors between theoretical prediction and numerical simulation are quantified. The relative error of displacement of the system and the relative error of the response amplitude are calculated. We end in §4 with conclusions.

2. Model and theoretical description

2.1 *Analysis of the model*

The dynamics of a fractional Mathieu–Duffing oscillator subjected to a biharmonic force and the distributed delay is governed by the equation of motion

$$\frac{\mathrm{d}^2x}{\mathrm{d}t^2}+\delta\frac{\mathrm{d}^\alpha x}{\mathrm{d}t^\alpha}+[a+g\cos(\Omega t)]x+bx^3 +\gamma\int_{-\infty}^{t}h(t-\tau)x(\tau)\mathrm{d}\tau=f\cos(\omega t), \tag{1}$$

where $\Omega \gg \omega$, $f \ll 1$. In the system, γ is the strength of time delay. The parameters a and b are the linear and nonlinear stiffness coefficient, respectively. α is the order of fractional damping, and this term is significant for the VR pattern. On the basis of the property of damping materials, α usually lies in the range of [0, 2] [51]. There are three common definitions for the fractional-order derivative operator, which are the Riemann–Liouville (R–L) definition, the Caputo definition and the Grünwald–Letnikov (G–L) definition [52,53]. The G–L definition is well-known for its simplicity in the discretisation of the fractional-order operators [30,31] and this definition is given by

$$\left.\frac{\mathrm{d}^\alpha f(t)}{\mathrm{d}t^\alpha}\right|_{t=kh}=\lim_{h\to 0}\frac{1}{h^\alpha}\sum_{j=0}^{k}(-1)^j\binom{\alpha}{j}f(kh-jh), \tag{2}$$

where the binomial coefficients are

$$\binom{\alpha}{0}=1,\quad \binom{\alpha}{j}=\frac{\alpha(\alpha-1)\cdots(\alpha-j+1)}{j!},\quad j\geq 1.$$

As a matter of fact, these three definitions are equivalent for a wide range of function classes which appear in practical applications [52].

The function $h(t)$ is the distributed delay kernel, which is the weight given to the population t time units ago and it satisfies $h(t) > 0$ together with the normalisation condition $\int_0^\infty h(t)\,\mathrm{d}t = 1$, which ensures that the steady states of model (1) are unaffected by the delay.

Following the ideal of Cushing [54], the weak kernel

$$h(t)=\sigma \mathrm{e}^{-\sigma t},\quad \sigma>0 \tag{3}$$

and the strong kernel

$$h(t)=\sigma^2 t\mathrm{e}^{-\sigma t},\quad \sigma>0 \tag{4}$$

are frequently encountered in the literature. $\delta > 0$ is the damping coefficient. In this paper, only eq. (1) with the weak kernel is investigated. The case with the strong kernel can be treated similarly. Consequently, the distributed time delay can be processed by setting

$$Z(t,x(t))=\int_{-\infty}^{t}h(t-\tau)x(\tau)\mathrm{d}\tau =\int_{-\infty}^{t}\sigma\mathrm{e}^{-\sigma(t-\tau)}x(\tau)\mathrm{d}\tau. \tag{5}$$

2.2 *Theoretical prediction*

When $\Omega \gg \omega$, the solution of eq. (1) can be achieved in the long time limit by $x(t) = X(t) + \Psi(t, \Omega t)$, where the periods of the slow variable X and the fast one Ψ are $2\pi/\omega$ and $2\pi/\Omega$, respectively. According to the method of direct partition of slow and fast motions, eq. (1) turns to

$$\begin{aligned}&\frac{\mathrm{d}^2X}{\mathrm{d}t^2} + \frac{\mathrm{d}^2\Psi}{\mathrm{d}t^2} + \delta\frac{\mathrm{d}^\alpha X}{\mathrm{d}t^\alpha} + \delta\frac{\mathrm{d}^\alpha \Psi}{\mathrm{d}t^\alpha} + aX + a\Psi + bX^3\\ &\quad + 3bX^2\Psi + 3bX\Psi^2 + b\Psi^3\\ &\quad + \gamma Z(t, X(t)) + \gamma Z(t, \Psi(t))\\ &= -Xg\cos(\Omega t) - \Psi g\cos(\Omega t) + f\cos(\omega t). \end{aligned} \tag{6}$$

As Ψ varies rapidly with time t, it is reasonable to ignore all nonlinear terms. Therefore, Ψ approximately satisfies the following linear equation:

$$\frac{\mathrm{d}^2\Psi}{\mathrm{d}t^2} + \delta\frac{\mathrm{d}^\alpha \Psi}{\mathrm{d}t^\alpha} + a\Psi + \gamma Z(t, \Psi(t)) = -Xg\cos(\Omega t). \tag{7}$$

By the theory of fractional derivatives [52,55], for $t \to \infty$, $\Psi(t) = A_H\cos(\Omega t + \Phi_H)$ is assumed to be the solution of (7). According to Appendix A, substituting Ψ and Z into eq. (7), one obtains

$$\begin{aligned}&A_H = \frac{Xg}{\mu}, \quad \mu = \sqrt{\mu_1^2 + \mu_2^2}, \quad \Phi_H = \arctan\frac{\mu_1}{\mu_2},\\ &\mu_1 = -\delta\Omega^\alpha \sin\left(\frac{\alpha\pi}{2}\right) + \frac{\gamma\sigma}{\sqrt{\Omega^2+\sigma^2}}\cos\theta,\\ &\mu_2 = a + \delta\Omega^\alpha\cos\left(\frac{\alpha\pi}{2}\right) + \frac{\gamma\sigma}{\sqrt{\Omega^2+\sigma^2}}\sin\theta - \Omega^2. \end{aligned} \tag{8}$$

Here,

$$\langle\Psi\rangle = \int_0^{2\pi/\Omega}\Psi\,\mathrm{d}t = 0,$$

$$\langle\Psi^2\rangle = \int_0^{2\pi/\Omega}\Psi^2\,\mathrm{d}t = \frac{1}{2}{A_H}^2,$$

$$\langle\Psi^3\rangle = \int_0^{2\pi/\Omega}\Psi^3\,\mathrm{d}t = 0$$

and

$$\int_0^{2\pi/\Omega}\Psi g\cos(\Omega t)\,\mathrm{d}t = \frac{1}{2}A_H g\cos(\Phi_H).$$

Then the slow variable X obeys the following motion according to eq. (6):

$$\begin{aligned}&\frac{\mathrm{d}^2X}{\mathrm{d}t^2} + \delta\frac{\mathrm{d}^\alpha X}{\mathrm{d}t^\alpha} + C_1X + C_2X^3\\ &\quad + \gamma Z(t, X(t)) = f\cos(\omega t), \end{aligned} \tag{9}$$

where

$$C_1 = a + \frac{g^2\cos(\Phi_H)}{2\mu}, \quad C_2 = b + \frac{3bg^2}{2\mu^2}.$$

Slow motions oscillate near the equilibrium point X^* of eq. (9) in the absence of harmonic force. X^* can be determined by denoting $Z(t, X(t)) = \sigma X(t)$, and we have

$$X_0^* = 0, \quad X_\pm^* = \pm\sqrt{-\frac{C_1+\gamma\sigma}{C_2}}. \tag{10}$$

Transformation $Y = X - X^*$ is executed, and eq. (9) turns to

$$\begin{aligned}&\frac{\mathrm{d}^2Y}{\mathrm{d}t^2} + \delta\frac{\mathrm{d}^\alpha Y}{\mathrm{d}t^\alpha} + \omega_r^2Y + 3C_2X^*Y^2 + C_2Y^3\\ &\quad + \gamma Z(t, Y(t)) = f\cos(\omega t), \end{aligned} \tag{11}$$

where $\omega_r = \sqrt{C_1 + 3C_2X^{*2}}$, which includes the effect of high-frequency oscillation owing to $g\cos(\Omega t)$ and represents the resonant frequency of the slow motion. For $f \ll 1$, the nonlinear term can be dropped under the assumption that $|Y| \ll 1$. Then, the following linear equation is given:

$$\frac{\mathrm{d}^2Y}{\mathrm{d}t^2} + \delta\frac{\mathrm{d}^\alpha Y}{\mathrm{d}t^\alpha} + \omega_r^2Y + \gamma Z(t, Y(t)) = f\cos(\omega t). \tag{12}$$

One gets $Y = A_L\cos(\omega t + \Phi_L)$ in the limit $t \to \infty$. Analogously, defining $\xi = \arctan(\sigma/\omega)$, the distributed delays feedback term can be expressed as

$$Z(t, Y(t)) = \frac{\sigma A_L}{\sqrt{\sigma^2+\omega^2}}\sin(\omega t + \Phi_L + \xi).$$

Following the steps used to determine A_H, we have

$$\begin{aligned}&A_L = \frac{f}{\sqrt{S}}, \quad S = S_1^2 + S_2^2, \quad \Phi_L = \arctan\frac{S_1}{S_2},\\ &S_1 = -\delta\omega^\alpha\sin\left(\frac{\alpha\pi}{2}\right) + \frac{\gamma\sigma}{\sqrt{\sigma^2+\omega^2}}\cos\xi,\\ &S_2 = \omega_r^2 + \delta\omega^\alpha\cos\left(\frac{\alpha\pi}{2}\right) + \frac{\gamma\sigma}{\sqrt{\sigma^2+\omega^2}}\sin\xi - \omega^2. \end{aligned} \tag{13}$$

To quantify the resonance character of the system, a target named response amplitude and labelled by Q will be used.

$$Q = \frac{A_L}{f} = \frac{1}{\sqrt{S}}. \tag{14}$$

2.3 *The numerical simulation*

Using the linear chain rule, system (1) can be transformed into the following equivalent system:

$$\begin{aligned}
\frac{\mathrm{d}^{\alpha}x}{\mathrm{d}t^{\alpha}} &= y(t),\\
\frac{\mathrm{d}^{\beta}y}{\mathrm{d}t^{\beta}} &= -\delta y(t) - [a + g\cos(\Omega t)]x(t) - bx^3(t)\\
&\quad -\gamma z(t) + f\cos(\omega t),\\
\frac{\mathrm{d}z}{\mathrm{d}t} &= \sigma x(t) - \sigma z(t),
\end{aligned} \tag{15}$$

where $\beta = 2 - \alpha$.

According to eq. (2), the simulations of eq. (15) can be acquired by

$$\begin{aligned}
x_{k+1} &= -\sum_{j=1}^{k} w_j^{(\alpha)} x_k + h^{\alpha}\cdot y_k,\\
y_{k+1} &= -\sum_{j=1}^{k} v_j^{(\beta)} y_k + h^{\beta}\\
&\quad \cdot\left[-\delta y_k - [a + g\cos(\Omega k)]x_k - bx_k^3 - \gamma z_k + \cos(\omega k)\right],\\
z_{k+1} &= z_k + h\cdot\sigma(x_k - z_k),
\end{aligned}$$

where

$$\begin{aligned}
\omega_0^{(\alpha)} &= v_0^{(\beta)} = 1, \quad \omega_j^{(\alpha)} = \left(1 - \frac{\alpha+1}{j}\right)\omega_{j-1}^{(\alpha)},\\
v_j^{(\beta)} &= \left(1 - \frac{\beta+1}{j}\right)v_{j-1}^{(\beta)}, \quad j = 1, 2, \ldots, k.
\end{aligned}$$

For the numerical simulation, the response amplitude can be calculated as follows [7]:

$$Q = \frac{\sqrt{B_s^2 + B_c^2}}{f}, \tag{16}$$

with B_s and B_c as

$$\begin{aligned}
B_s &= \frac{2}{nT}\int_0^{nT} x(t)\sin(\omega t)\mathrm{d}t,\\
B_c &= \frac{2}{nT}\int_0^{nT} x(t)\cos(\omega t)\mathrm{d}t,
\end{aligned}$$

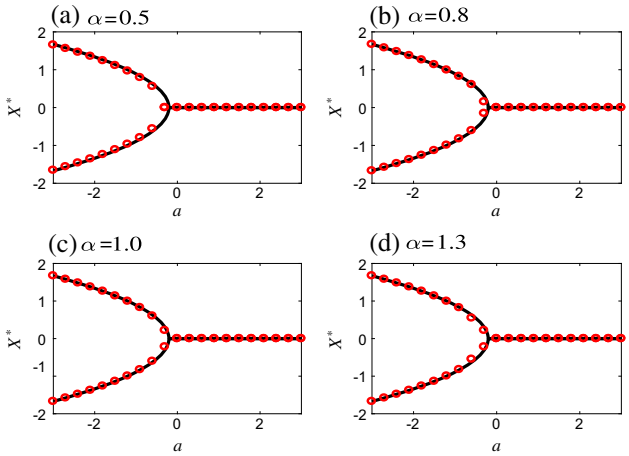

Figure 1. The pitchfork bifurcation induced by the parameter a. The simulation parameters are: $f = 0.1, g = 1$, $\omega = 0.5, \Omega = 10, \gamma = 0.2, b = 1, \delta = 0.5$ and $\sigma = 1$.

where $T = 2\pi/\omega$, n is a positive integer which should be large enough to guarantee the accuracy of the numerical results.

3. Analysis of resonance

3.1 *The distributed delay*

Yang *et al* [38] proposed a numerical method to simulate different types of local bifurcation of the equilibria,

$$X^* = \frac{1}{rT}\int_0^{rT} x(t)\mathrm{d}t, \tag{17}$$

where $T = 2\pi/\omega$ and r is a large integer number, and we still analyse the equilibrium points by this method. In this subsection, the errors between theoretical prediction and numerical simulation are quantified. The relative error is defined as

$$e_X = \frac{\sum_i |x_{\mathrm{T}}(i) - x_{\mathrm{N}}(i)|}{\sum_i x_{\mathrm{N}}(i)} \times 100\%, \tag{18}$$

where $x_{\mathrm{T}}(i)$ and $x_{\mathrm{N}}(i)$ are respectively the theoretical prediction and numerical simulation of the system displacement.

Yang *et al* [38] have comprehensively analysed the relationship between the equilibrium point and damping coefficients and fractional damping. In this study, when the parameter b is positive, the term C_2 is also positive. When $a > 0$, we also have $C_1 > 0$ and there is no pitchfork bifurcation. When $a < 0$, the term C_1 may change its sign with the change of fractional order. When the value of nonlinear stiffness coefficient $b = 1$, combined with the previous analysis, the results shown

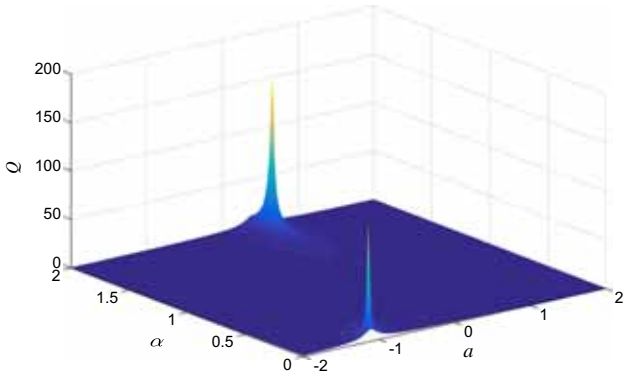

Figure 2. The analytical result of Q vs. α and a.

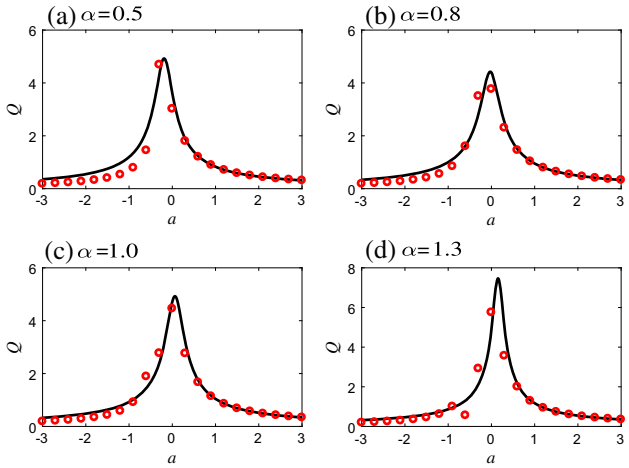

Figure 3. The resonance induced by the linear stiffness coefficient for different values of the fractional order.

in figure 1 can be obtained. For different values of the fractional order, the analytical prediction and numerical simulation formula of equilibrium points are shown in figure 1. The continuous lines are plotted by the analytical method according to eq. (10), the discrete points are drawn by the numerical simulation according to eq. (17). It is found that the numerical results are in good agreement with the analytical predictions. As for the displacement in this model, a few papers verify the accuracy of prediction and numerical method by quantisation error. To further illustrate this effect, we calculate the relative error of displacement. When $\alpha = 0.5, 0.8, 1.0$ and 1.3 in figure 1, the relative errors of displacement x are 5.30, 1.80, 1.14, 1.69%, respectively. It is informed that the relative errors of displacement are minute and the numerical method is accurate. In other words, it is reasonable to accept the theoretical prediction and numerical simulation methods. Another important fact is that the bifurcation behaviour occurs in the diagram. The subcritical pitchfork bifurcation induced by a is clearly displayed for different fractional order. As the stable equilibrium point changes from non-trivial to trivial, subcritical pitchfork bifurcation occurs. In figure 1, $a = 0$ is the critical point of pitchfork bifurcation.

Next, we shall analyse the influence of system parameters on the response amplitude (Q). When we choose a as the control parameter, Q vs. α and a are plotted in figure 2. For a fixed fractional order, Q vs. a presents a resonance phenomenon. For a fixed a, the magnitude of the resonance peak will change by increasing the fractional order.

To further discuss the effect of a on the resonance phenomenon much more clearly, we plotted figure 3. In figures 3a–3d, the maximum of Q is 4.9273, 4.4232, 4.9273, 7.4666, respectively, and at resonance peak, the linear stiffness coefficients are -0.19, -0.03, 0.06 and 0.15. To maximise Q, along with the rising of fractional order, a has been increased. Next, the maximum of Q is different when $\alpha < 1$ and $\alpha > 1$. Yang *et al* [38] indicated that for a larger value of α, the magnitude of Q is larger too. However, when the fractional order is far away from $\alpha = 1$, the response may have a large magnitude (see figure 3). This suggests that the research in distributed delay in this oscillator is very interesting.

Similar to eq. (18), the relative error of Q is

$$e_Q = \frac{\sum_i |Q_{\mathrm{T}}(i) - Q_{\mathrm{N}}(i)|}{\sum_i Q_{\mathrm{N}}(i)} \times 100\%, \tag{19}$$

where $Q_{\mathrm{T}}(i)$ and $Q_{\mathrm{N}}(i)$ are respectively the theoretical prediction and numerical simulation of the system output. Then in figure 3 the relative errors of Q are 22.29, 16.42, 13.49 and 21.83% in light of eq. (19), respectively. Obviously, due to two linearisations in theoretical derivation, the relative error of Q is larger than the relative error of equilibrium point. In fact, the method of direct partition of slow and fast motions is sensitive to external excitation. So the calculation accuracy is low. However, because of its simplicity and rapidity, this method is widely used in engineering field. In addition, there are average method, perturbation method, multiscale method and so on [56].

As is known to all, we can determine the response frequency through the ω–α–Q curve. This is of great significance in the engineering field. The analytical result of Q vs. α and ω are plotted in figure 4. Compared to other results [38], the variation trend of the response amplitude is similar, but its value varies greatly. This shows that introducing discrete time delay into the model can effectively improve the system output. As ω approaches 1, Q is large. And when ω continues to increase, Q decreases instead. Particularly, the maximum of Q is 3.4433, 2.4063, 2.4254 and 3.2750 at $\omega = 1.2$, 1.09, 1

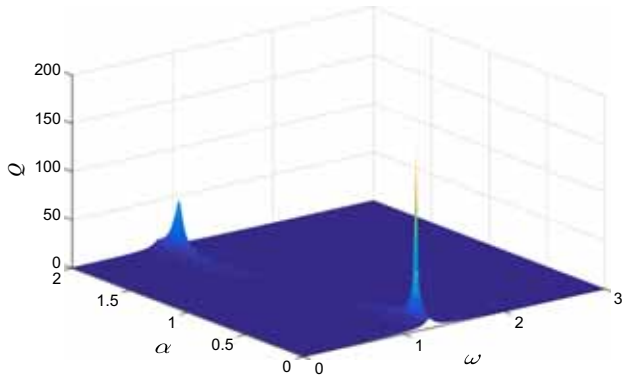

Figure 4. The analytical result of Q vs. α and ω.

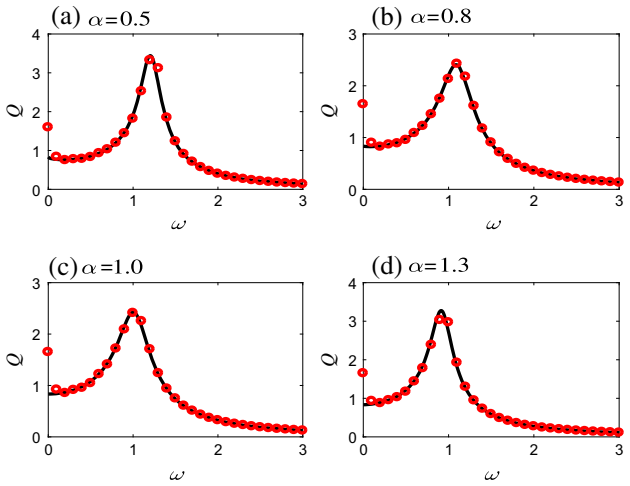

Figure 5. The resonance frequency induced by low-frequency for different values of α.

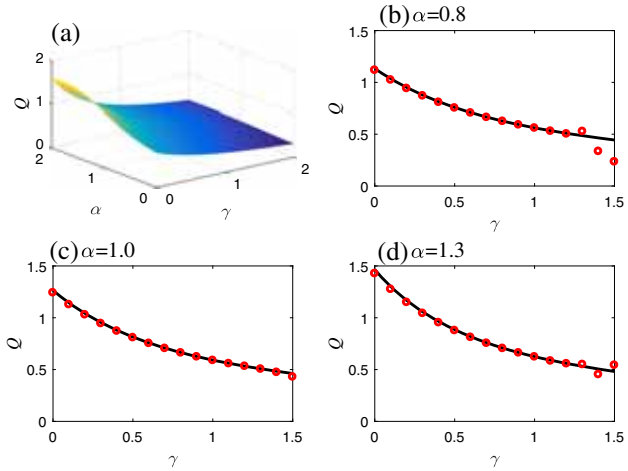

Figure 6. The response amplitude induced by γ for different values of α.

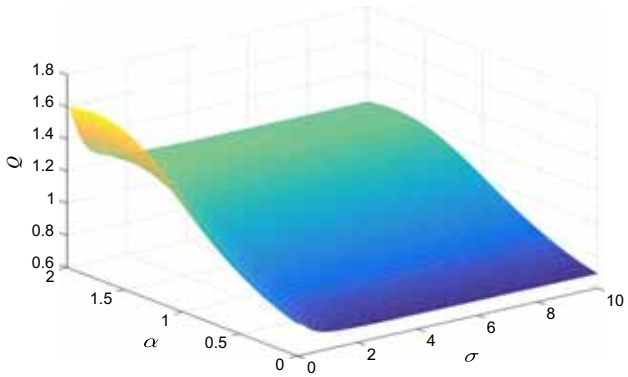

Figure 7. The response amplitude induced by σ and α.

and 0.91 in figures 5a–5d, respectively. With the increase of fractional order, ω decreases when Q reaches the maximum value. When we compare these four subgraphs, it is clearly seen that Q gets bigger as α goes away from 1, and the relative errors of Q are 4.28, 2.36, 2.43 and 4.47% according to eq. (19). In a statistical sense, there is no doubt that the theoretical prediction and the numerical simulation are consistent.

Thereafter, we study the effect of delay strength (γ) of the model. On the one hand, in figure 6a, when γ is fixed, the output of the system increases with the expansion of fractional order. That is, $Q = 0.9510$, 1.0513 and 1.1797 at $\gamma = 1$ in figures 6b–6d, respectively. On the other hand, for a fixed α, Q decreases by increasing γ in figures 6b–6d. In other words, excessive time delay strength can change the system. The greater the strength of time delay, the smaller the effective output of the system, which is consistent with the actual situation. What will happen to the system if, instead of a distributed delay in the form of a weak kernel, there is a fixed delay in the fractional Mathieu–Duffing oscillator? It also makes us interested in this type of research. The specific research is in the next subsection. Last but not the least, it can be clearly seen that when $\gamma < 1$, the numerical results are very consistent with the analytical prediction.

The response amplitude vs. σ and α are plotted according to the analytical result in figure 7. As we said, σ is the damping coefficient. In light of eq. (5) and the weak kernel definition, σ is also the rate parameter in the exponential distribution. Consequently, the effect of σ on the system displacement is consistent with its role in the exponential distribution. However, for a fixed fractional order α, Q decreases by increasing σ. In the meantime, when $\sigma < 1$, Q changes rapidly with the increase of σ. But when $\sigma > 1$, Q does not change greatly with the increase of σ. This change is similar to the effect of rate parameter on exponential distribution.

3.2 *The fixed time delay*

In order to better illustrate the distributed delay effect on the model, we introduce the following model:

$$\frac{\mathrm{d}^2x}{\mathrm{d}t^2} + \delta\frac{\mathrm{d}^\alpha x}{\mathrm{d}t^\alpha} + [a + g\cos(\Omega t)]x + bx^3 + \gamma x(t-\tau) = f\cos(\omega t), \tag{20}$$

where τ represents the fixed time delay and γ is the strength of the linear time delay feedback. Different from eq. (1), the delay is fixed above. Similar to the theoretical prediction in §2.2, we can obtain these main results:

$$A_H^\# = \frac{Xg}{\mu^\#},$$

$$\mu^\# = \sqrt{\mu_{11}^2 + \mu_{21}^2}, \quad \theta_H^\# = -\arctan\frac{\mu_{11}}{\mu_{21}},$$

$$\mu_{11} = \left(\gamma\sin(\Omega\tau) - \delta\Omega^\alpha\sin\left(\frac{\alpha\pi}{2}\right)\right)^2,$$

$$\mu_{21} = \left(a - \Omega^2 + \gamma\cos(\Omega\tau) + \delta\Omega^\alpha\cos\left(\frac{\alpha\pi}{2}\right)\right)^2,$$

$$C_1^\# = a + \frac{g^2\cos\theta_H^\#}{2\mu^\#}, \quad C_2^\# = b + \frac{3bg^2}{2\mu^{\#2}},$$

$$X_0^* = 0, \quad X_\pm^* = \pm\sqrt{-\frac{C_1^\#+\gamma}{C_2^\#}}, \quad \omega_r^\# = C_1^\# + 3C_2^\# X^{*2},$$

$$S^\# = \sqrt{S_{11}^2 + S_{21}^2}, \quad A_L^\# = \frac{f}{S^\#}, \quad \theta_L^\# = \arctan\frac{S_{11}}{S_{21}},$$

$$S_{11} = \left(\gamma\sin(\omega\tau) - \delta\omega^\alpha\sin\left(\frac{\alpha\pi}{2}\right)\right)^2,$$

$$S_{21} = \left(\omega_r^\# - \omega^2 + \gamma\cos(\omega\tau) + \delta\omega^\alpha\cos\left(\frac{\alpha\pi}{2}\right)\right)^2,$$

$$Q^\# = \frac{A_L^\#}{f}. \tag{21}$$

Taking a and α as control parameters, we plotted figures 8 and 9. First, contrary to figure 2, Q vs. a presents not only one resonance, but two resonances in figure 8. It is demonstrated that the fixed delay is beneficial to the occurrence of new resonance. In addition, similar to figure 2, we found that resonance mostly occurred near $a = 0$. For a fixed value of a, Q changes rapidly with the increase of fractional order. In particular, when α approaches 2, the system output is nearly 350. This shows once again that the artificial introduction of fixed time delay in the oscillator can greatly increase the system output. In fact, the time delay is

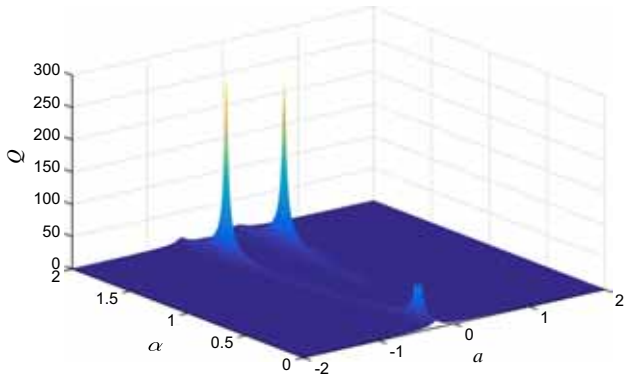

Figure 8. The analytical result of Q vs. α and a. The simulation parameters are: $\delta = 0.5, b = 1, \gamma = 0.2$, $\omega = 0.5, \Omega = 10, f = 0.1, g{=}1, \tau = 1$.

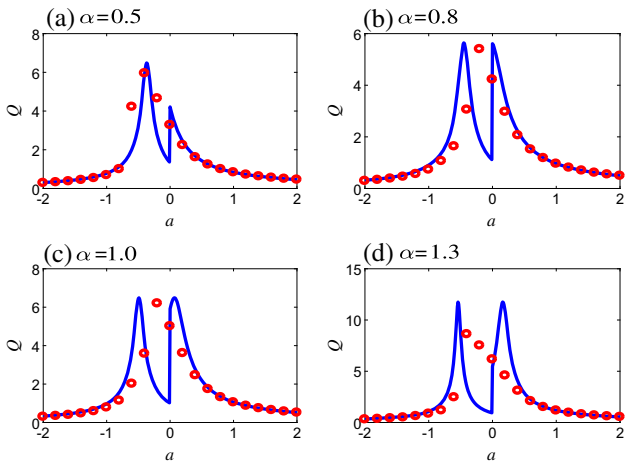

Figure 9. The resonance induced by a for different values of α.

widespread in real system. Yang *et al* [38] studied that when $\alpha < 1$, the curve Q–a is in a single-resonance mode, and for the case $\alpha \in [1, 2)$, the curve Q–a is in a double-resonance mode. Compared with the conclusions in ref. [38], there are two peaks in figure 9. However, in figures 9b–9d, the heights of the peaks are the same. We analyse that different equilibrium points change the magnitude of resonance peak in figure 9a. At the same time, the resonance value of $\alpha > 1$ was much higher than that of $\alpha < 1$. In order to verity the correctness of the method of direct partition fast and slow motions used in model (20), we calculated the relative error according to eq. (19) in figure 9. For $\alpha = 0.5, 0.8, 1.0$ and 1.3, the relative error is 18.23, 31.75, 30.37, 54.49%, respectively. The numerical simulation in figure 9 does not match with the theoretical prediction results as well as those in figure 3. But in figures 1, 3, 5 and 6 for model (1), we confirmed that the analysis method is reasonable. Therefore, we suspect that this error is due to the fixed time delay.

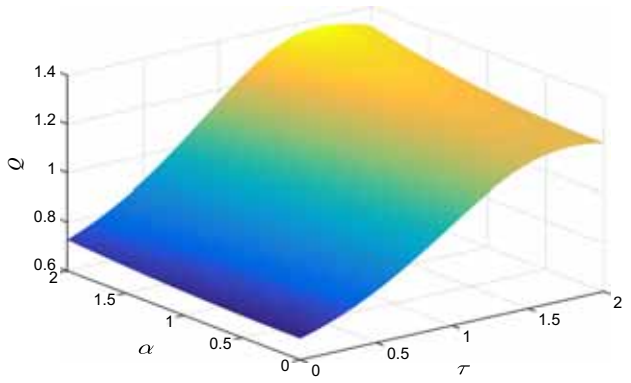

Figure 10. The resonance induced by τ for different values of α.

The response amplitude Q vs. α and τ is given in figure 10. For a fixed value of α, the output of the system increases by increasing τ when $\tau < 1.2$, but Q decreases by increasing τ when $\tau > 1.2$. Too much time delay may damage the system. It is not the same as in model (1). In fractional Mathieu–Duffing oscillator, the structure of the system may be destroyed by fixed delays. Through the above analysis, we find that, unlike this fractional oscillator with no time delay [38], the system has abundant phenomena when $\tau = 1$. Comparing figures 6, 7 and 10, it can be found that the fixed delay and the distributed delay have no significant influence on the oscillator.

4. Conclusion

In this present work, we have investigated vibration dynamics in two time-delayed fractional Mathieu–Duffing oscillator. The two kinds of delays are the distributed delay and the fixed time delay. In §2, a fractional Mathieu–Duffing oscillator with the distributed delay is given. Based on vibration mechanism, the theoretical expression of Q is obtained by utilising the method of separation of slow and fast motions. In §3, numerical simulation and theoretical prediction of equilibrium points and values of Q are studied separately. Usually, they are in good agreement, but there is no quantisation error between these two calculations. In this paper, we introduce the relative error between the theoretical prediction and numerical simulation. Moreover, the relative error is not only reflected in the displacement of the system, but also in the system output. The results indicate that we have reason to believe that this theoretical analysis is statistically correct. The subcritical pitchfork bifurcation induced by a is clearly shown for different fractional order. Therefore, the effects of fractional order, linear stiffness coefficient, low-frequency signal, time delay intensity and damping coefficient on a Mathieu–Duffing oscillator with distributed delay are studied successively. The influence of linear stiffness coefficient and low-frequency signal on this system are similar, and the fractional order can alter the value of Q. When the fractional order is far away from $\alpha = 1$, the response may have a large magnitude. To better illustrate the distributed delay effect on the model, we also introduce a fixed delay in this system. It can be found that the distributed delay has significant influence on this oscillator compared to fixed delay. Compared to other results [38], we conclude that introducing time delay into the model can effectively improve the output of the system. That is, there are many more different dynamical properties in the distributed delay oscillator than that in the fixed delay one. These results give us a better understanding of the influence of time delay on VR of a fractional Mathieu–Duffing oscillator. By studying these new results, we hope to control the system more effectively.

Acknowledgements

This work was partially funded by the National Natural Science Foundation of China under Grant No. 11202120 and the Fundamental Research Funds for the Central Universities under No. GK201901008.

Appendix A. An appendix section

In light of eq. (5) and $x = X + \Psi$,

$$\begin{aligned} Z(t, x(t)) &= \int_{-\infty}^{t} \sigma \mathrm{e}^{-\sigma(t-\tau)}(x(\tau))\,\mathrm{d}\tau \\ &= \int_{-\infty}^{t} \sigma \mathrm{e}^{-\sigma(t-\tau)}(X(\tau) + \Psi(\tau))\,\mathrm{d}\tau \\ &= Z(t, X(t)) + Z(t, \Psi(t)). \end{aligned} \tag{A.1}$$

For $\Psi(t) = A_H \cos(\Omega t + \Phi_H)$, then

$$\begin{aligned} Z(t, \Psi(t)) &= \int_{-\infty}^{t} \sigma \mathrm{e}^{-\sigma(t-\tau)}\Psi(\tau)\,\mathrm{d}\tau \\ &= \sigma A_H \int_{-\infty}^{t} \mathrm{e}^{-\sigma(t-\tau)} \cos(\Omega\tau + \Phi_H)\,\mathrm{d}\tau \\ &= \sigma A_H \mathrm{e}^{-\sigma t} \int_{-\infty}^{t} \mathrm{e}^{\sigma\tau} \cos(\Omega\tau + \Phi_H)\,\mathrm{d}\tau. \end{aligned} \tag{A.2}$$

According to the divisional integration method, the integral value in (A.2) is

$$\int_{-\infty}^{t} \mathrm{e}^{\sigma\tau}\cos(\Omega\tau+\Phi_H)\,\mathrm{d}\tau = \frac{\mathrm{e}^{\sigma t}}{\sqrt{\Omega^2+\sigma^2}}\sin\Big(\Omega t+\Phi_H+\arctan\frac{\sigma}{\Omega}\Big).$$

We have

$$\mathrm{Z}(t,\Psi(t)) = \frac{\sigma A_H}{\sqrt{\Omega^2+\sigma^2}}\sin(\Omega t+\Phi_H+\theta) \qquad (A.3)$$

where

$$\theta = \arctan\frac{\sigma}{\Omega}.$$

References

[1] R Benzi, A Sutera and A Vulpianni, *J. Phys. A* **14**, L453 (1981)
[2] G Litak and M Borowiec, *Nonlinear Dyn.* **77**, 681 (2014)
[3] J H Yang, M A F Sanjuán, H G Liu, G Litak and X Li, *Commun. Nonlinear Sci. Numer. Simul.* **41**, 104 (2016)
[4] M Gitterman, *J. Phys. A* **34**, L355 (2001)
[5] V N Chizhevsky, E Smeu and G Giacomelli, *Phys. Rev. Lett.* **91**, 220602 (2003)
[6] V N Chizhevsky and G Giacomelli, *Phys. Rev. A* **71**, 011801 (2005)
[7] P S Landa and P V E McClintock, *J. Phys. A*: **33**, L433 (2000)
[8] B Deng, J Wang, X L Wei, K M Tsang and W L Chan, *Chaos* **20**, 013113 (2010)
[9] Y M Qin, J Wang, C Men, B Deng and X L Wei, *Chaos* **21**, 023133 (2011)
[10] J B Sun, B Deng, C Liu, H T Yu, J Wang, X L Wei and J Zhao, *Appl. Mech. Rev.* **37**, 6311 (2013)
[11] J P Baltanás, L Lopez, I I Blechman, P S Landa, A Zaikin, J Kurths and M A F Sanjuán, *Phys. Rev. E* **67**, 066119 (2003)
[12] D L Hu, J H Yang and X B Liu, *Commun. Nonlinear Sci. Numer. Simul.* **17**, 1031 (2012)
[13] D L Hu, J H Yang and X B Liu, *Comput. Biol. Med.* **45**, 80 (2014)
[14] A Daza, A Wagemakers, S Rajasekar and M A F Sanjuán, *Commun. Nonlinear Sci. Numer. Simul.* **18**, 400 (2013)
[15] V N Chizhevsky and G G Iacomelli, *Phys. Rev. E* **70**, 062101 (2004)
[16] C G Yao and M Zhan, *Phys. Rev. E* **81**, 061129 (2010)
[17] C J Fang and X B Liu, *Chin. Phys. Lett.* **29**, 050504 (2012)
[18] J H Yang and X B Liu, *J. Phys. A* **43**, 122001 (2010)
[19] T L M D Mbong, M Siewe and C Tchawoua, *Mech. Res. Commun*. **78**, 13 (2016)
[20] F Yang and K Q Zhu, *Theor. Appl. Mech. Lett.* **1**, 012007 (2011)
[21] F C Meral, T J Royston and R Magin, *Commun. Nonlinear Sci. Numer. Simul.* **15**, 939 (2010)
[22] Y Q Chen, R T Sun, A H Zhou and N Zaveri, *J. Vib. Control* **14**, 9 (2008)
[23] K B Oldham, *Adv. Eng. Softw.* **41**, 9 (2010)
[24] F Mainardi, Fractional calculus, in: *Fractals and fractional calculus in continuum mechanics* (Springer, 1997) pp. 291–348
[25] Y A Rossikhin and M V Shitikova, *Appl. Mech. Rev.* **63**, 010801 (2010)
[26] T L M D Mbong, M Siewe and C Tchawoua, *Commun. Nonlinear Sci. Numer. Simul.* **22**, 228 (2015)
[27] M Li, *Math. Prob. Eng.* **2010** (2010)
[28] O P Agrawal, *Nonlinear Dyn.* **38**, 323 (2004)
[29] S Das and I Pan, *Fractional-order signal processing: Introductory concepts an applications* (Springer Science & Business Media, 2011)
[30] J H Yang, *Chin. Phys. Lett.* **29**, 104501 (2012)
[31] J H Yang and H Zhu, *Chaos* **22**, 013112 (2012)
[32] M Li, *Symmetry* **10**, 40 (2018)
[33] N F Pedersen, M R Samuelsen and K Særmark, *J. Appl. Phys.* **44**, 5120 (1973)
[34] V Kaajakari and A Lal, *Appl. Phys. Lett.* **85**, 3923 (2004)
[35] M A Mironov, P A Pyatakov, I I Konopatskaya, G T Clement and N I Vykhodtseva, *Acoust. Phys.* **55**, 567 (2009)
[36] M H El Ouni, N B Kahla and A Preumont, *Eng. Struct.* **45**, 244 (2012)
[37] H Plat and I Bucher, *J. Sound. Vib.* **333**, 1408 (2014)
[38] J H Yang, M A F Sanjuán and H G Liu, *Eur. Phys. J. B* **88**, 310 (2015)
[39] Z J Chen and L J Ning, *Pramana – J. Phys.* **90**: 49 (2018)
[40] Z L Yang and L J Ning, *Pramana – J. Phys.* **92**: 89 (2019)
[41] R J Yatawara, R D Neilson and A D S Barr, *J. Sound. Vib.* **297**, 962 (2006)
[42] M Belhaq and S M Sah, *Commun. Nonlinear. Sci. Numer. Simul.* **13**, 1706 (2008)
[43] A Fidlin and J J Thomsen, *Int. J. Non-Linear. Mech.* **43**, 569 (2008)
[44] J J Thomsen, *J. Sound. Vib.* **311**, 1249 (2008)
[45] B Horton, J Sieber, J M T Thompson and M Wiercigroch, *Int. J. Non-Linear Mech.* **46**, 436 (2011)
[46] L Mokni, M Belhaq and F Lakrad, *Commun. Nonlinear. Sci. Numer. Simul.* **16**, 1720 (2011)
[47] R H Huan, W Q Zhu, F Ma and Z H Liu, *Shock Vib.* **2014**, 1 (2014)
[48] Y L Song and Y H Peng, *Appl. Math. Comput.* **181**, 1745 (2006)
[49] J Wu, X S Zhan, X H Zhang and H L Gao, *Chin. Phys. Lett.* **29**, 050203 (2012)
[50] A Mesbahi, M Haeri, M Nazari and E A Butcher, *Int. J. Control* **88**, 622 (2015)
[51] R Caponetto, G Dongola, L Fortuna and I Petráš, (World Scientific, 2010)
[52] I Podlubny, *Fractional differential equations: An introduction to fractional derivatives, fractional differential*

equations, to methods of their solution and some of their appliactions (Elsevier, 1998) Vol. 198

[53] C A Monje, Y Q Chen, B M Vinagre, D Y Xue and V Feliu Batlle, *Fractional-order systems and controls: Fundamentals and applications* (Springer Science & Business Media, 2010)

[54] J M Cushing, *J. Math. Biol*. **4**(3), 257 (1977)

[55] I I Blekhman, *Vibrational mechanics: Nonlinear dynamic effects, general approach, applications* (World Scientific, 2000)

[56] J H Yang, *Diffraction and resonance in fractional-order systems* (Science Press, Beijing, 2017)